2022 IEEE 5th International Conference on Soft Robotics (RoboSoft)
April 4-8, 2022, Edinburgh, UK

In-Hand Object Recognition with Innervated Fiber Optic Spectroscopy for Soft Grippers

Nathaniel Hanson[1], Hillel Hochsztein[1], Akshay Vaidya[1], Joel Willick[1], Kristen Dorsey,[1], Taşkın Padır[1]

***Abstract*— Previous work in material sensing with soft robots has focused on integrating flexible force sensors or optical waveguides to infer object shape and mass from experimental data. In this work, we present a novel modular sensing platform integrated into a hybrid-manufactured soft robot gripper to collect and process high-fidelity spectral information. The custom design of the gripper is realized using 3D printing and casting. We embed full-spectrum light sources paired with lensed fiber optic cables within an optically clear gel, to collect multi-point spectral reflectivity curves in the Visible to Near Infrared (VNIR) segment of the electromagnetic spectrum. We introduce a processing pipeline to collect, clean, and merge multiple spectral readings. As a demonstration of sensor capabilities, we gather sample readings from several similarly-shaped and textured items to show how spectroscopy enables explainable differentiation between objects. The integration of spectroscopic data presents a promising new sensing modality for soft robots to understand the material composition of grasped items, facilitating numerous applications for food-processing and manufacturing.**

***Index Terms* – Soft sensors and actuators, additive manufacturing, perception for grasping and manipulation, spectral sensing**

I. INTRODUCTION

Compliant soft robotic grippers are highly effective at handling a variety of object geometries, including pliable objects or those with delicate surfaces. Soft robot manipulators are characterized by a grasp strategy which more evenly distributes applied pressure [1]. This adaptable grasping form mirrors the versatility of human hands and their ability to change shape to securely lift and carry objects. However, current robot grippers struggle to identify what they have grasped. Humans are proficient at inferring object class and similarity from the object shape, size, weight, and material type. In our interactions with everyday objects, we leverage past encounters with similar objects to reinforce our categorizations and develop inferences into how to handle unknown items [2]. However, we are imbued with a somatosensory system capable of responding to varied tactile stimuli far exceeding the current capabilities of robotic grasping [3].

Recent advances in quantifying object material properties for robot applications have contributed techniques based on human sensory capabilities, including touch and vision. Specifically in prior work involving direct contact with objects (presented in detail in Section II), much attention has been given to visual sensing or texture estimation via an elastomeric sensor mounted on a parallel-plate gripper [4], [5], [6], [7]. Our goal in this research is to demonstrate visible to near infrared (VNIR) spectroscopy in tandem with manipulation by a soft gripper, as a step towards improved in-hand object recognition.

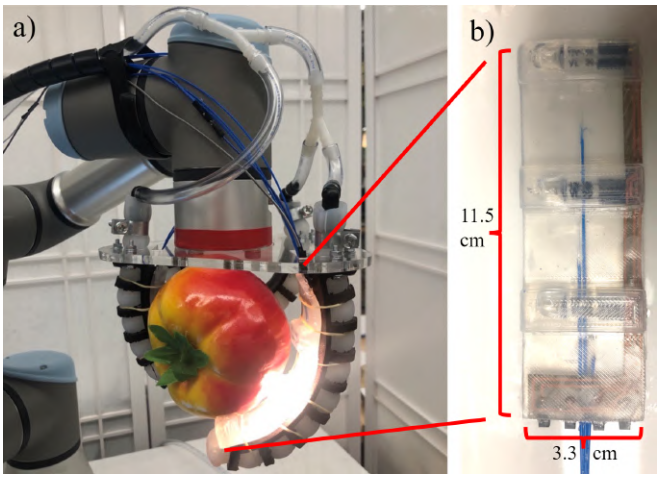

Fig. 1: a) Soft Gripper with innervated fiber optic cables and encapsulated full spectrum light sources mounted to a 6 Degrees of Freedom robotic arm. b) Profile of gripper pad.

We present the design and manufacturing process for a reconfigurable soft gripper, as pictured in Fig. 1, capable of collecting VNIR spectral data from multiple points on grasped objects in real-time, as the gripper closes to its final form. VNIR spectroscopy yields additional information about chemical composition that is not available through tactile sensing alone. Our approach is grounded in observations that many organic and inorganic materials reflect distinct quantities of incident light across the spectrum allowing their identification by a spectral signature [8], [9].

Our gripper design is modular with each subsystem comprising a flexible electronic circuit and illumination source. The current setup consists of a soft robotic gripper in a parallel 3-finger configuration. Furthermore, given the modular framework different configurations can be utilized as per the application requirements. This allows the robot to collect successive spectral samples from multiple points on the object and develop a map of the grasped object's material type and chemical characteristics [10]. This knowledge is useful in not only discriminating between classes, but also in understanding intra-class variation. In particular, we measure the reflected photon counts in the wavelength range (λ) 350 - 1150 nm. The paper's contributions are as follows:

*This research is supported by the National Science Foundation under Award Number 1928654.

[1]Institute for Experiential Robotics, Northeastern University, Boston, Massachusetts, USA.
Nathaniel Hanson is the corresponding author.
hanson.n@northeastern.edu

2022 IEEE 5th International Conference on Soft Robotics (RoboSoft) | 978-1-6654-0828-8/22/$31.00 ©2022 IEEE | DOI: 10.1109/ROBOSOFT54090.2022.9762166

- A design for an exoskeleton-based, pneumatically-actuated soft robotic gripper with a modular sensor tray.
- Techniques to embed fiber optic cables within elastomeric gel and ensure unimpeded, diffuse full-spectrum light to manipulated objects.
- An algorithm to collect multi-point spectral information and demonstrate how it is used to distinguish objects by their spectral signatures.

The paper is organized as follows. Section II outlines current work in robot material sensing through visual and haptic approaches, focused on soft robotic manipulators. In Section III we discuss the material selection to create a soft robotic gripper with fiber optic capabilities and highlight the fabrication procedure in Section IV. Section V details an algorithm and system architecture to acquire and merge multiple spectral signatures using sequentially triggered readings from within the gripper fingers. Section VI shows a practical demonstration of the system in collecting readings from objects of similar geometries with a discussion in Section VII. Finally, Section VIII discusses our results and future opportunities for spectral sensing with soft robots.

II. RELATED WORK

A. Grasped Material Identification

Previous approaches to grasped material identification fall under two general categorizations: contact-based and contact-free. Contact-free methods commonly employ computer vision to label individual pixels or patches of images, although such methods are subject to illumination noise and are limited by the material resolution available [11], [12], [13].

Elastomeric sensors are the current state-of-the-art system in contact-based material estimation. They measure surface topography and contact forces through deformation of a contact gel imaged by a small, high-resolution camera [4], [5], [6]. The imaged gel deformation is an input to a Convolutional Neural Network (CNNs), allowing deep learning models to learn grasping strategies for many objects. [6]. Elastomeric tactile sensing has been restricted to rigid robotic manipulators, as their designs require fixed spatial placement of illuminating Light Emitting Diodes (LEDs) relative to the surface gel; such an assumption is difficult to maintain for flexible grippers. Increasing the size and deformation capabilities of the sensing area through an air-regulated bladder has been shown to be a reasonable compromise between wholly flexible and rigid grippers [7].

Work with compliant grippers has focused on identifying objects by their shape and force as observed by the manipulator when lifting them. Zhao et al. developed a technique to manufacture optical waveguides - a lossy light conduit capable of measuring deformation by comparing light transmitted to a terminal sensor with the unimpeded transmission to a photodetector [14], [15]. Bai et al. created a fabrication process to make these waveguides from stretchable gels and tri-color dye doped regions sporting spatial resolution of ≈ 1 cm [16]. Although these waveguides provide coarse estimates of the object shape and size, they fail to understand the underlying material of the grasped object, as finer textures and composition cannot be differentiated.

B. Spectroscopy

Field spectroscopy is a developing discipline, particularly within the area of robotics. Previously, [21] utilized commercial spectrometers to differentiate between generalized material classes, such as metal, plastic, wood, paper, and fabric with the introduction of a neural network architecture and improved their findings with visual-spectral fusion [22]. The same group later used this mounted spectrometer to quantify object penetrability for autonomous tool construction [23].

In the agriculture domain, [24] designed and constructed a gripper with two spectral probes and accelerometers to simultaneously measure the spectral profile and hardness of a mango as inputs to a ripening index. However, since the gripper could only grip round items of a certain size, it does not generalize to multiple grasping scenarios.

In our prior work [25], we developed a parallel plate gripper with an integrated spectral probe and endoscope camera. Combining online data processing and a nonlinear Support Vector Machine (SVM) machine learning model, the gripper demonstrated the capability to distinguish between visually similar real (organic) and fake (plastic/polystyrene) fruits with an accuracy of 96.41% in a 32-class decision problem.

III. MATERIALS

A. Soft Gripper Selection

From the literature, we selected a hybrid manufactured soft robotic finger using casting and 3D printing [26] as the base for our sensing platform. We chose this design since it represented a robust, platform to add a sensing array. Additionally, the 3D printed exoskeleton adds lateral and torsion stability in all but the target direction of motion. This torsion resistance is important for the integrity of the embedded electronics, which can break electrical contacts when twisted. We consider these core benefits of this exoskeleton gripper:

- Faster fabrication time as a bladder, exoskeleton and sensor tray can be fabricated in parallel.
- Materials of the bladder and exoskeleton may be varied for a tailor-made actuator with desired characteristics.
- 3D printing allows for the rapid modification and iteration of exoskeleton designs as required.

The gripper design process has been driven by a set of design specifications, including: (1) Handling objects of size 0-8.5 cm in diameter; (2) Collecting continuous spectral data at a rate of 10 Hz in the wavelength range 400 - 1100 nm; (3) Collecting three readings per finger using an in-situ illumination source; (4) Lifting objects ≤ 2.0 kg.

B. Spectrometer Specifications

To collect spectral readings, we utilize a BLUE-Wave miniature spectrometer (StellarNet, Inc.). The device's small form factor (13.42 cm $\times$ 8.81 cm $\times$ 3.12 cm) and signal-to-noise ratio of 1000:1 adds to its reliability as a platform for integration with a co-robot manipulator. The system is

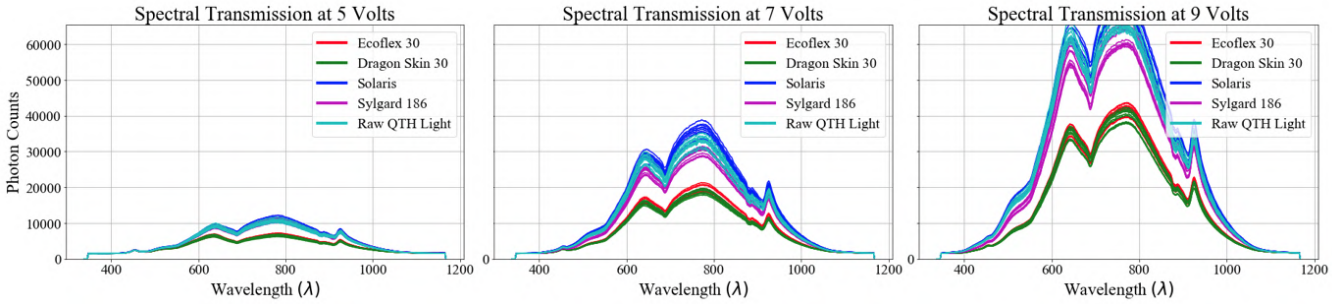

Fig. 2: Visible to Near Infrared (VNIR) light transmission of elastomeric gels with QTH bulb at different applied voltages. Note: 16-bit photodetector saturates at 2^{16} photons per integration period.

consistently utilized by chemists and biologists, and provides data transmission and configuration over USB [27], [28]. The device is calibrated by the manufacturer, and its internal detector is sensitive to the range of 350 - 1150 nm. Light is introduced to the spectrometer via a single input slit (width 100 μm) and diffracted across a grating to a silicon-based detector. This counts incident photons in the localized wavelength range. The spectrometer in this setup is designed to be replaceable with other spectrometers, providing additional wavelength range or sensitivity as dictated by the application.

C. Elastomeric Gel Selection

We considered three key characteristics for the sensor grip pad: (1) flexibility, (2) hardness, and (3) optical clarity. We evaluated four commonly used silicone elastomers: Solaris (Smooth-On Inc.) [17], Dragon Skin 30 (Smooth-On Inc.) [18], EcoFlex 30 (Smooth-On Inc.) [19], and Sylgard 186 (Dow Chemical Company) [20]. We prioritized optical clarity since the fibers need minimally obstructed light to ensure adequate characterization of grasped materials. Using the StellarNet Spectrometer, we measured reflected light from a Quartz Tungsten Halogen (QTH) bulb reflected against a white reference standard (Spectralon) through an 8 mm thick piece of each gel at a distance of 20 cm to avoid saturation. We observed the intensity of the reflected light at three different voltages, as shown in Fig. 2. Sylgard and Solaris produce greater responses than the raw light in some collections since the material acted as a lens and provided a slight focusing effect increasing the number of detected photons. We avoid increasing the voltage beyond 10 V here, as the increased voltage corresponds to increased illuminance and sensor saturation.

Based on the material properties detailed in Table I and results from Fig. 2 we selected Sylgard 186 as the base material for the optics sensor tray. It offers adequate compressive and tensile strength while coming in as a close second to Solaris in terms of optical clarity. We note that while Solaris exhibits nearly unimpeded light transmission at all voltages across the spectrum, it manifests a brittleness in demolding and a tendency to allow small surface imperfections or abrasions to propagate through the width of the cast volume when bent. This observation reinforces the manufacturer's recommendation that Solaris is chiefly designed for static encapsulation and not regular bending.

D. Full Spectrum Illumination

For VNIR spectroscopy to accurately measure reflected light, incident light must be representative of the wavelengths being measured. Normal LEDs provide only a limited spectral illumination source ($\approx$ 20nm Full Width Half Maximum (FWHM) [29] and an array covering the necessary spectrum with LEDs would prove unnecessarily complex. In previous research, we used a fiber optic bundle to deliver light from a QTH bulb in close proximity to the signal fiber. However, such a bundle requires additional protective layers to preserve the fiber arrangement, reducing its flexibility. In this research the QTH bulbs (Thorlabs) are embedded directly into the elastomeric finger grip pads. This strategy jointly enables us to illuminate grasped objects in a wide range of ambient lighting conditions and deliver localized diffuse light for individual fiber acquisition.

QTH bulbs suffer from the known challenge of high operating temperatures [30]. In order to minimize heat accumulation caused by continuous operation, the bulbs are pulsed in a sequential fashion whenever a grasping procedure is initialized. As shown in Fig. 3, we tested the bulb temperature rise by applying a sequence of voltages to each bulb: 12 V, the maximum voltage recommended by the manufacturer, for 5 seconds, 0 V for 5 seconds, repeatedly over 3 hours measuring the ambient and surface temperature of the bulb with an infrared thermometer (Adafruit). The bulb temperature plateaus at 35°C in Fig. 3 - within range of Sylgard's safe working temperature. This also establishes an upper threshold for bulb heat. A single anomalous sensor

TABLE I: Quantitative comparison of properties for different silicon-based elastomeric gels. Bold indicates best attribute.

Gel Type	Shore A Hardness	Tensile (PSI)	Tear -die B (kN/m)	Elongation at Break (%)	Temp. Range (°C)	Clarity
Solaris [17]	15	180	Not Available	290	-100 – 205	**Clear**
Dragon Skin 30 [18]	**30**	**500**	**18.9**	364	**-53 – 232**	Translucent
Ecoflex 30 [19]	**30**	200	6.66	**900**	**-53 – 232**	Translucent
Sylgard 186 [20]	24	305	7.0	255	-45 – 200	**Clear**

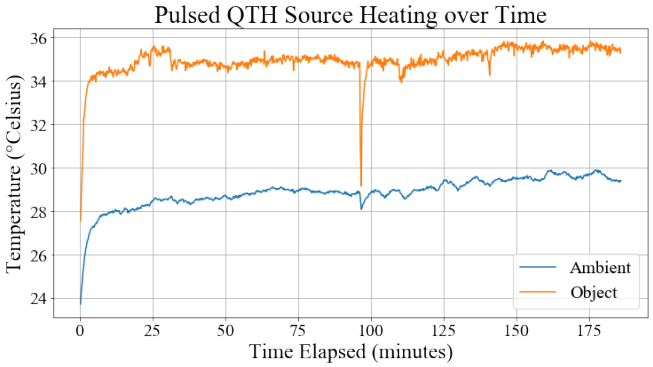

Fig. 3: Quartz Tungsten Halogen (QTH) source heat accumulation in surface and environment ambient temperatures over time as measured by an infrared thermometer.

reading near 100 elapsed minutes is not consequential to the thermal stability. Fig. 4 shows a finite element simulation in SOLIDWORKS demonstrating the additional thermal dissipation properties presented by placing the bulbs in gel as well as the concentration points of surface heat.

IV. Fabrication

A. Fiber Optic Cables

Spectrometers contain complex electrical components which are not easily miniaturized, nor made flexible since they rely on a predefined geometry to split light into component wavelengths. Fiber optic probes are used to make spectroscopy more dynamic by leveraging the glass fiber's total internal reflectance to route light into the spectrometer inlet slit, thus separating the photodetector from the point of interest. Fiber optics' inherent flexibility, up to a bend radius defined by the thickness and cable cladding, makes them ideal candidates for inclusion in a flexible gripper.

Although excellent conduits for a NIR spectrum, fiber optic strands have a limited numerical aperture (NA) which defines the sine of the largest angle that light offset from the fiber core will enter the length. To overcome this challenge, we utilize specialized lensed fibers (LaseOptics Corp.), diagrammed in Fig. 5, capable of transmitting light from 350 - 2200 nm. These fibers are nearly identical in form and function to a standard optics-grade fiber, but contain a microscopic ball lens and $45°$ cleave with metal

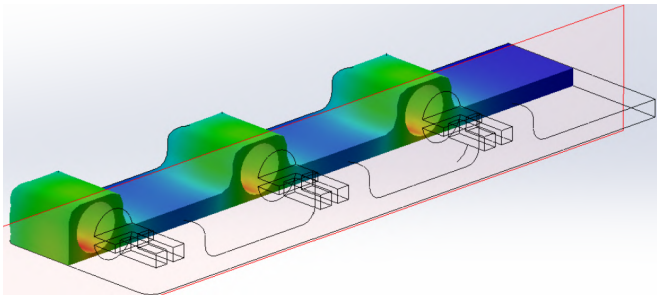

Fig. 4: Thermal dispersion of embedded light source heat in a soft gripper pad. The highest concentration of heat is indicated in red, opposite the main object contact surface. Blue indicates cooler surface temperature.

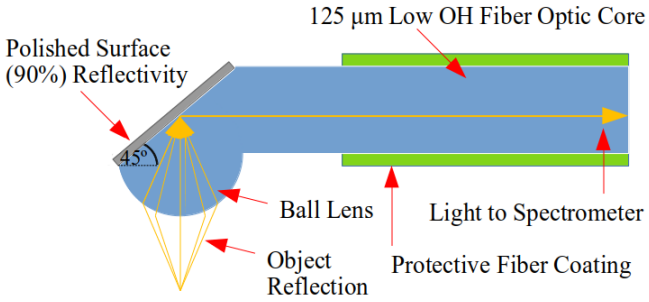

Fig. 5: Lensed fiber optic cable cross-section diagram.

surface polish to change the end aperture of the cable to be perpendicular to the fiber length. In effect, this allows us to run fiber through the length of the finger while still collecting measurements from grasped objects.

B. Flexible Circuitry

The power circuitry for the QTH lamps is a printed circuit board (PCB) fabricated on flexible, copper-clad FR4, which is itself embedded in the gripper pad. We designed the board in EAGLE, laser etched the prototypes on a UV laser (LPKF Protolaser U4) and soldered components by hand. Since Sylgard 186 has a volume resistivity of $4.98 \times 10^{15}\ \Omega cm$, it effectively protects the circuit board, meaning no additional soldermask or conformal coating is necessary to prevent shorts. In addition to conveying electrical power to the lamps, the circuit board also acts as a scaffold, holding the lamps in the correct position during the casting process. The board was oriented with its most bendable axis parallel to the primary bending direction of the gripper, and its surface area was minimized to limit the amount of bending stiffness.

C. Gripper Pad Configuration

The gripper pad consists of alternating thick and thin segments of constant width. In addition to adding surface texture and tack, the thicker sections are large enough to encapsulate the QTH lamps while the thin portions add only enough stiffness to protect the innervated fibers. The Sylgard 186 was cast in 3D printed molds, made of Onyx™ (nylon-carbon fiber matrix) on a Markforged X7. Sylgard 186 is highly viscous (66700 cP) while in its pot state, which makes vacuum degassing very difficult. We supplement degassing with curing in a heated, pressurized chamber ($65.6°$ C at $\approx$ 80 PSI) to compress the inset gas bubbles for the duration of the cure. This resulted in an optical clarity similar to that of degassed Solaris. The thermal stability of the Onyx™ prevents deformation in the molding chamber.

Because of the fragility of the encased elements, as well as the Sylgard 186's low tear strength, unstructured demolding (such as bending and pulling) caused significant damage to the gripper pads. Rather than using a mold release agent, which would mar the surface finish (and therefore optical quality) of the pad, we designed a mold with integrated ejectors. These not only served as mold geometry but also minimized shearing forces in demolding. We further smoothed the mold with Sulfur-free modeling clay to minimize surface texture left by the 3D printing process.

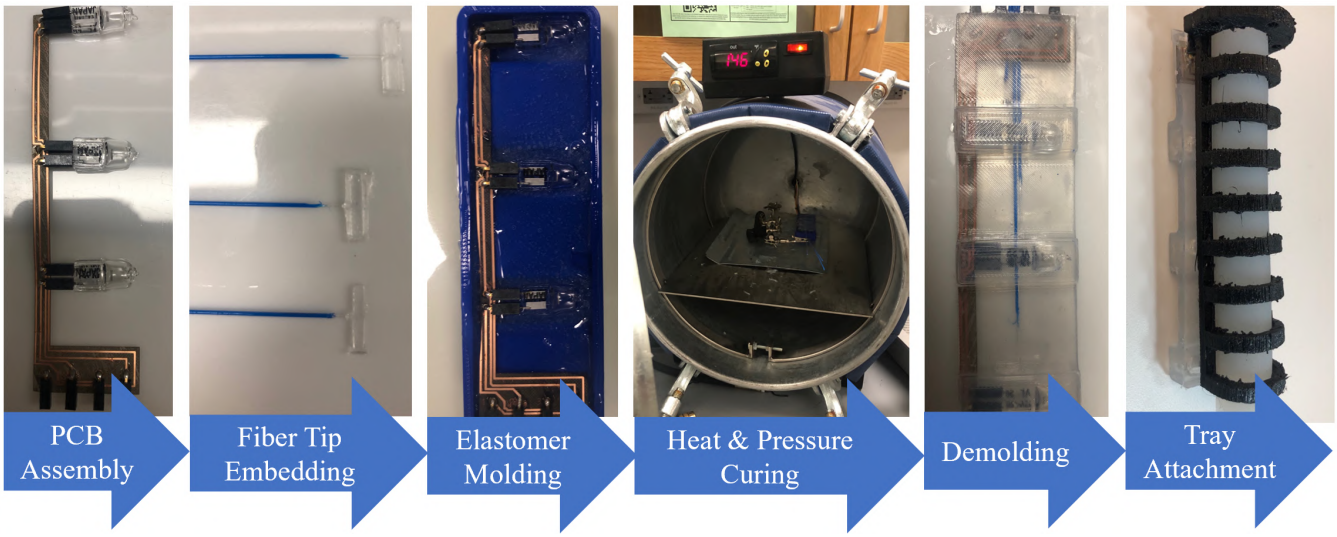

Fig. 6: Fabrication steps for fiber optic sensor tray and attachment to soft gripper finger.

D. Fiber Innervation

To ensure coverage of grasped items, we placed fiber optic receptors at the center of each thin section of the grip pad. This spacing ensures that the QTH lamps do not saturate the signal and causes a natural air gap between the lensed end of the fiber and the item of interest; allowing light to be reflected into the lens. Since the lensed end is perpendicular to the axis of the fiber, orientation of the fiber during casting is particularly important as even minor angular deviations can affect the quantity of light focused into the limited NA of the fiber. The fibers have a 125 μm bare fiber diameter, meaning that the contact area for clamping is small relative to the overall width of the gripper pad. The possibility for torsion must be accounted for both in the clamped region of the fiber, and in the region between the clamped point and the lens. To improve distributed contact in the fiber clamping, we used swatches of Ecoflex 30 placed along the jaws of the clamp, which protects the fibers from point compression while increasing friction. Furthermore, we innervated the fibers in two separate stages:

1) We cast "wings" fused to the tip of each fiber. By using a small mold, we could clamp the fiber closer to the lensed end, limiting possible torsion. We attached a light source to the fiber so we could see the lensed end's orientation and aligned the beam in the mold. We then poured and cured the wings.
2) We placed the winged fibers in their positions, centered between the gripper pads containing the QTH bulbs, and poured the Sylgard a second time with all of the encapsulated components. Since the wings are larger and resistant to twisting, a single clamp could hold the fibers in place without concern about rotational alignment of the fibers during the second cure.

Fig. 6 shows the end-to-end fabrication for a single gripper.

E. Assembly

The completed gripper pads (with electronics and fibers) attach to the flexible gripper's 3D printed skeleton with elastic bands. This skeleton is mounted to the adapter plate, which connects to the robot (Universal Robotics UR3e) and routes the electrical, optical, and fluid connections.

- **Electronics:** The PCBs terminate in wired connections that lead to a relay board connected to a power source. This allows any combination of lamps to be illuminated programmatically via a microcontroller (Arduino Uno).
- **Optics:** The optical fibers terminate with SMA-905 connections to a switch (Agiltron). This device uses a series of micro-electro-mechanical systems (MEMS) reflectors to switch the fiber connected to the spectrometer. Both the switch and the spectrometer are operated electronically via serial connection.
- **Pneumatics:** The flexible gripper's inflatable bladders are connected to a pressurized air line through a regulator (Parker-Watts R374-02GB). Increasing the maximal pressure increases the angle of finger actuation. This can be done either programmatically or manually.

V. DATA ACQUISITION

Fig. 7 outlines the physical and electrical linkages necessary to actuate and acquire data from the gripping system. Spectral data requires initial calibrations to remove system noise from the readings. We take two readings: the dark count d, defining the system noise when no ambient light is present, and w, defining the total reflectance of a white reference standard. This step is performed once per device, since local lighting conditions are controlled within the grasp of the gripper, with reflected QTH light dominating the signal. We also record an empty grasp baseline reading, and use the Spectral Angle Mapper [31] similarity measure from hyperspectral imaging literature to determine if a grasped object is proximal to the fiber end. Similarity is scored from $(0°, 90°)$.

$$\text{SAM(X,R)} = \cos^{-1} \frac{\sum XR}{\sqrt{(\sum (X)^2 \sum (R)^2)}} \tag{1}$$

where X is the current fiber reading and R is the empty reference signal. We compare the SAM score against a threshold and only use the sample reading if the readings

Algorithm 1 Multi-Point Spectral Data Acquisition

Input: integration time τ, dark count calibration d, white reference calibration w, maximum grasp pressure p_{max}, empty grasp reading g, difference threshold δ
Initialize:
$relay(f) \leftarrow LOW$ for all f $\in$ Fiber Array
$p_{applied} \leftarrow 0$
$counts(f) \leftarrow 0$ for all f $\in$ Fiber Array
$N(f) \leftarrow 0$, for all f $\in$ Fiber Array
while $p_{applied} < p_{max}$ **do**
  for f $\in$ Fiber Array **do**
    $relay(f) \leftarrow HIGH$
    $raw\_data \leftarrow$ read_spectrometer(f, τ)
    $cal\_data \leftarrow \frac{raw\_data - d}{w - d}$
    if SAM(cal_data,g) $> \delta$ **then**
      $counts(f) \leftarrow cal\_data$
      $N(f) \leftarrow N(f) + 1$
    end if
    $relay(f) \leftarrow LOW$
  end for
end while
return counts, N

are dissimilar. This approach can also be used to compare successful grasped samples with known spectral signatures. The complete grasping algorithm is given in Algorithm 1.

VI. DEMONSTRATION

To demonstrate the system is capable of collecting spectral data we selected three items of similar size, shape, and texture. Namely we used a tennis ball, a polystyrene and plastic faux pear, and a polystyrene and plastic faux pomegranate. We selected these items since current state-of-the-art waveguides would likely produce similar optical responses as the gripper conformed to the round object geometry. Using the innervated fingers, we collected a baseline empty grasp, where no object is held, considered in Algorithm 1 as g. We operated the QTH lamps at 9.8 V: an empirically selected value from the bulb temperature study and from observed saturation of the spectrometer at higher operating voltages. We measured the spectral response through the embedded fibers with an integration time of 1.0 second per scan to ensure maximal absorption of light by the silicon detector. Including a switching time of 0.5 seconds, the scan time over the 9 sensors in three fingers totaled 14 seconds. We scan averaged and normalized the readings against Spectralon total reflectance and dark signal calibrations samples. Results were averaged across the samples collected for each finger.

VII. DISCUSSION

Visually, from these plotted spectral reflectivity curves in Fig 8, we see how each item has its own characteristic spectral curve as a function of the wavelength of incident light. Even for items of the same base material, namely the pear and the pomegranate, the varying mixtures of dyes and pigments are sufficient to trigger a distinctive response. From 400 nm - 700 nm, the spectral profiles show a significant

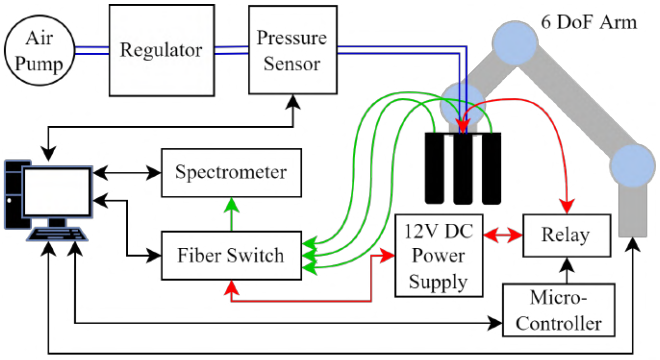

Fig. 7: System architecture for actuation of soft gripper and acquisition of spectral readings. Color-coded system connections include: Red = Electrical Power, Blue = Pneumatic, Green = Fiber Optic, and Black = Data.

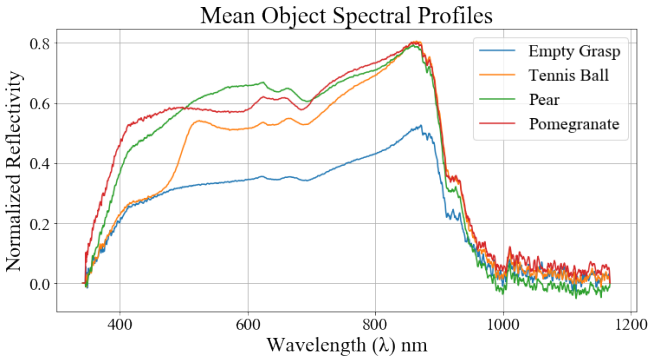

Fig. 8: Collected object samples using gripper pad with normalized spectral reflectivity. The curves are averaged across an acquisition cycle using a single finger in a full contact position.

divergence originating in the visible light portion of the spectrum. For example, the tennis ball profile shows an dramatic increase between 500 and 600 nm, indicating the ball has a strong yellow-green color profile. The spectral profiles at wavelengths less than 780 nm can be used for precise object color reconstruction, which itself might be a useful means to distinguish between multiple objects, or understand the composition and quality of multiple instances of the same object class.

At longer wavelengths, the NIR range, material properties start to become more apparent. As we have observed in prior work, synthetic materials exhibit a large peak in spectral intensity around 900 nm [25]. The silicon-based photodetector ideally has quantum efficiency, the likelihood an incident photon triggering an electrical response, of at least 40% in the visible range. There is significant system noise between 900-1100 nm. This is partially attributable to intrinsic attenuation caused by the silica in the fiber optic cables themselves and decreasing quantum efficiency of the detector as the system reaches its limit at 1150 nm.

VIII. CONCLUSION

In this research, we presented a novel material-sensing capability for soft robotic grippers. Our gripper builds upon our prior work in hybrid fabrication methods for exoskeleton-

based gripper fingers and rigid spectral sensing. We detailed a fabrication procedure to innervate an elastomeric gripper pad with flexible electronics and lensed fiber optic cables for measurement of material composition. Our work contributes a unique capability to recognize objects beyond shape, weight, and texture.

In the near future, we plan to refine the mold design to optimize the fabrication process and improve gel optical clarity. Additionally, we plan to switch to a fiber diameter of 250 μm to increase the number of photons transmitted in each scan, which will decrease the total acquisition time. Increasing the diameter might preclude the usage of lensed fibers due to manufacturing constraints, but micro-prisms appear to be a good alternative to redirect light into the fiber core. With an improved system, we plan to continue validation on a wider variety of object classes and material types. Future opportunities also include the fusion of optical waveguides with spectroscopic sensing for further refinement for finger position. A single system which measures both material composition and finger position holds promise. Our work demonstrates spectroscopy provides a boon in both recognizing and understanding the chemical-physical properties of in-hand objects.

ACKNOWLEDGMENTS

The authors are grateful to Charles DiMarzio for his excellent engineering advice and suggestions in the selection of optics components. Mark Zolotas provided useful feedback in the composition of this paper.

REFERENCES

[1] J. Shintake, V. Cacucciolo, D. Floreano, and H. Shea, "Soft robotic grippers," *Advanced Materials*, vol. 30, no. 29, p. 1707035, 2018.

[2] G. Buckingham, J. S. Cant, and M. A. Goodale, "Living in a material world: how visual cues to material properties affect the way that we lift objects and perceive their weight," *Journal of neurophysiology*, vol. 102, no. 6, pp. 3111–3118, 2009.

[3] V. E. Abraira and D. D. Ginty, "The sensory neurons of touch," *Neuron*, vol. 79, no. 4, pp. 618–639, 2013.

[4] R. Li and E. H. Adelson, "Sensing and recognizing surface textures using a gelsight sensor," in *Proceedings of the IEEE Conference on Computer Vision and Pattern Recognition*, 2013, pp. 1241–1247.

[5] Z. Wang, Z. Li, B. Wang, and H. Liu, "Robot grasp detection using multimodal deep convolutional neural networks," *Advances in Mechanical Engineering*, vol. 8, no. 9, p. 1687814016668077, 2016.

[6] A. C. Abad and A. Ranasinghe, "Visuotactile sensors with emphasis on gelsight sensor: A review," *IEEE Sensors Journal*, vol. 20, no. 14, pp. 7628–7638, 2020.

[7] A. Alspach, K. Hashimoto, N. Kuppuswamy, and R. Tedrake, "Soft-bubble: A highly compliant dense geometry tactile sensor for robot manipulation," in *2019 2nd IEEE International Conference on Soft Robotics (RoboSoft)*. IEEE, 2019, pp. 597–604.

[8] S. Serranti, A. Gargiulo, and G. Bonifazi, "Classification of polyolefins from building and construction waste using nir hyperspectral imaging system," *Resources, Conservation and Recycling*, vol. 61, pp. 52–58, 2012.

[9] R. Kokaly, R. Clark, G. Swayze, K. Livo, T. Hoefen, N. Pearson, R. Wise, W. Benzel, H. Lowers, R. Driscoll, *et al.*, "Usgs spectral library version 7 data: Us geological survey data release," *United States Geological Survey (USGS): Reston, VA, USA*, 2017.

[10] B. M. Nicolai, K. Beullens, E. Bobelyn, A. Peirs, W. Saeys, K. I. Theron, and J. Lammertyn, "Nondestructive measurement of fruit and vegetable quality by means of nir spectroscopy: A review," *Postharvest biology and technology*, vol. 46, no. 2, pp. 99–118, 2007.

[11] G. Schwartz and K. Nishino, "Recognizing material properties from images," *IEEE transactions on pattern analysis and machine intelligence*, vol. 42, no. 8, pp. 1981–1995, 2019.

[12] S. Bell, P. Upchurch, N. Snavely, and K. Bala, "Material recognition in the wild with the materials in context database," in *Proceedings of the IEEE conference on computer vision and pattern recognition*, 2015, pp. 3479–3487.

[13] R. W. Fleming, "Visual perception of materials and their properties," *Vision research*, vol. 94, pp. 62–75, 2014.

[14] H. Zhao, K. O'Brien, S. Li, and R. F. Shepherd, "Optoelectronically innervated soft prosthetic hand via stretchable optical waveguides," *Science robotics*, vol. 1, no. 1, p. eaai7529, 2016.

[15] C. B. Teeple, K. P. Becker, and R. J. Wood, "Soft curvature and contact force sensors for deep-sea grasping via soft optical waveguides," in *2018 IEEE/RSJ International Conference on Intelligent Robots and Systems (IROS)*. IEEE, 2018, pp. 1621–1627.

[16] H. Bai, S. Li, J. Barreiros, Y. Tu, C. R. Pollock, and R. F. Shepherd, "Stretchable distributed fiber-optic sensors," *Science*, vol. 370, no. 6518, pp. 848–852, 2020.

[17] *Clear Silicone Encapsulating Rubber*, Smooth-On, Inc., 9 2021.

[18] *Dragon Skin Series Addition Cure Rubber Compounds*, Smooth-On, Inc., 4 2021.

[19] *Super-Soft, Addition Cure Silicone Rubbers*, Smooth-On, Inc., 2 2021.

[20] *SYLGARD 186 Silicon Elastomer*, The Dow Chemical Company, 2017, 11-1253-01 C.

[21] Z. Erickson, N. Luskey, S. Chernova, and C. C. Kemp, "Classification of household materials via spectroscopy," *IEEE Robotics and Automation Letters*, vol. 4, no. 2, pp. 700–707, 2019.

[22] Z. Erickson, E. Xing, B. Srirangam, S. Chernova, and C. C. Kemp, "Multimodal material classification for robots using spectroscopy and high resolution texture imaging," in *2020 IEEE/RSJ International Conference on Intelligent Robots and Systems (IROS)*. IEEE, 2020, pp. 10 452–10 459.

[23] L. Nair, N. S. Srikanth, Z. M. Erickson, and S. Chernova, "Autonomous tool construction using part shape and attachment prediction." in *Robotics: Science and Systems*, 2019.

[24] V. Cortés, C. Blanes, J. Blasco, C. Ortiz, N. Aleixos, M. Mellado, S. Cubero, and P. Talens, "Integration of simultaneous tactile sensing and visible and near-infrared reflectance spectroscopy in a robot gripper for mango quality assessment," *Biosystems Engineering*, vol. 162, pp. 112–123, 2017.

[25] N. Hanson, T. Kelestemur, D. Erdogmus, and T. Padir, "Pregrasp object material classification by a novel gripper design with integrated spectroscopy," 2021, under peer review.

[26] M. B. Oliveira, A. Lurie, D. Ewen, P. Long, T. Padir, and S. M. Felton, "Hybrid fabrication of a soft bending actuator with casting and additive manufacturing," in *International Design Engineering Technical Conferences and Computers and Information in Engineering Conference*, vol. 59230. American Society of Mechanical Engineers, 2019, p. V05AT07A015.

[27] R. Pourdarbani, S. Sabzi, D. Kalantari, and J. I. Arribas, "Non-destructive visible and short-wave near-infrared spectroscopic data estimation of various physicochemical properties of fuji apple (malus pumila) fruits at different maturation stages," *Chemometrics and Intelligent Laboratory Systems*, vol. 206, p. 104147, 2020.

[28] A. L. Jenkins, M. W. Ellzy, and L. C. Buettner, "Molecularly imprinted polymer sensors for detection in the gas, liquid, and vapor phase," *Journal of Molecular Recognition*, vol. 25, no. 6, pp. 330–335, 2012.

[29] M. H. Weik, "Spectral width," in *Computer Science and Communications Dictionary*. Boston, MA: Springer US, 2001, pp. 1633–1633.

[30] R. Jenkins, B. Aldwell, S. Yin, M. Meyer, A. Robinson, and R. Lupoi, "Energy efficiency of a quartz tungsten halogen lamp: Experimental and numerical approach," *Thermal Science and Engineering Progress*, vol. 13, p. 100385, 2019.

[31] X. Liu and C. Yang, "A kernel spectral angle mapper algorithm for remote sensing image classification," in *2013 6th International Congress on Image and Signal Processing (CISP)*, vol. 2. IEEE, 2013, pp. 814–818.